Eur. Phys. J. A (2023) 59:127
https://doi.org/10.1140/epja/s10050-023-01042-3

THE EUROPEAN PHYSICAL JOURNAL A

Regular Article - Experimental Physics

Average photonuclear cross section measurements for the ^{141}Pr, ^{160}Gd and ^{162}Er isotopes and compared with Geant4 simulations

G. T. Bholane, T. S. Ganesapandy, S. H. Patil, S. S. Dahiwale, V. N. Bhoraskar, S. D. Dhole[a]

Department of Physics, S. P. Pune University, Pune 411007, India

Received: 11 July 2022 / Accepted: 22 May 2023

Communicated by Navin Alahari.

Abstract The flux weighted average cross sections of the ^{141}Pr(γ,n)^{140}Pr, ^{160}Gd(γ,n)^{159}Gd and ^{162}Er(γ,n)^{161}Er nuclear reactions induced by 10 and 15 MeV energy bremsstrahlung photons are measured with offline gamma spectrometry. The cross sections are reported with detailed uncertainties in the associated parameters. The measured cross sections are compared with the theoretical cross sections calculated using TALYS 1.95 code for eight different gamma strength functions. The average cross sections are also compared with the Geant4 Monte Carlo simulations of the nuclear reactions induced by bremsstrahlung photons. The measured cross sections are important for the nuclear database and nuclear astrophysics research.

1 Introduction

The experimentally measured cross sections for many rare earth elements for photon induced reactions are not available on the EXFOR [1] database. The interest for the measurements of the cross section for these reactions has been increased in the recent years due to availability of various photon sources. The photo nuclear reactions in the giant dipole region (GDR) are important for neutron production estimation at the nuclear facilities. Photo nuclear reactions for medium and heavy nuclei are also important for the study of stellar nucleosynthesis. The heavy neutron deficient nuclei called as p-nuclei are produced in the stellar environment either by successive addition of protons to a nucleus or by removing neutrons from the nucleus though nuclear reactions accompanied by subsequent beta decays. This process is termed as p-process or γ-process in nuclear astrophysics. These astrophysical p-processes can be studied through various (γ,n) nuclear reactions in a laboratory with sufficiently high photon flux. The photo nuclear cross sections are also useful for the estimation of the stellar photoneutron rates [2].

The element praseodymium has one stable isotope ^{141}Pr (100%), gadolinium has six stable isotopes ^{154}Gd (2.18%), ^{155}Gd (14.8%), ^{156}Gd (20.47%), ^{157}Gd (15.65%), ^{158}Gd (24.84%) and ^{160}Gd (21.86%) and erbium also has six stable isotopes ^{162}Er (0.139%), ^{164}Er (1.601%), ^{166}Er (33.503%), ^{167}Er (22.869%), ^{168}Er (26.978%) and ^{170}Er (14.91%). The ^{162}Er nucleus studied in this work is a p-nucleus. The cross sections for the reaction ^{141}Pr(γ,n)^{140}Pr has been reported by a few authors to EXFOR. However, most of the data was reported before 1992 and only one author has reported in 2006. The previous authors have not used HPGe detector for the measurement of the induced activity in the samples. Some of them have used ^{3}He or BF_3 neutron detector to measure the secondary neutrons emitted from the samples. The secondary neutrons are moderated by polyethene or paraffin before detection. Other authors have used NaI(Tl) detectors for gamma spectrometry, which have poor energy resolution. There is a significant loss of precision in these techniques. These results are helpful for photoneutron folding technique to determine the photoneutron spectra generated at electron accelerators.

In the present work, the flux weighted average cross sections of ^{141}Pr(γ,n)^{140}Pr, ^{160}Gd(γ,n)^{159}Gd and ^{162}Er(γ,n)^{161}Er nuclear reactions induced by 10 and 15 MeV end point energy bremsstrahlung photons are reported. A medical LINAC is used for the irradiation of the samples in the present work. So far, the cross sections of these reactions have not been reported in the EXFOR database, except for the cross section of ^{160}Gd(γ,n)^{159}Gd reported by Ghosh et al. [3] at 10 MeV and ^{162}Er(γ,n)^{161}Er reported by Vagena et al. [4] at 14 MeV bremsstrahlung photons and compared with TALYS evaluations. In the present work, the measured cross sections are compared with the theoretical effective cross sections calculated with TALYS 1.95 [5] nuclear code for eight

[a] e-mail: sanjay@physics.unipune.ac.in(corresponding author)

Published online: 11 June 2023

Table 1 The nuclear spectroscopic data for the different radioisotopes produced in the present work [9–12]

Nuclide	Half-life	Decay mode	Eγ (keV)	Iγ (%)
^{140}Pr	3.39 ± 0.01 m	ec β + (100%)	1596.1 ± 0.2	0.49 ± 0.04
^{159}Gd	18.479 ± 0.004 h	β − (100%)	363.543 ± 0.0018	11.78 ± 0.05
^{161}Er	3.21 ± 0.03 h	ec β + (100%)	826.6 ± 0.1	64 ± 4
^{196}Au	6.1669 ± 0.0006 d	ec β + (93%) β − (7%)	355.73 ± 0.05	87 ± 3

Table 2 Experimental details of the irradiation, cooling and counting time for the nuclear reactions along with the threshold energy of the nuclear reactions

Reaction	Endpoint energy (MeV)	Irradiation time (s)	Cooling time (s)	Counting time (s)	Threshold energy E_{th} (MeV)
^{141}Pr(γ,n)^{140}Pr	10	300	25	300	9.399
^{160}Gd(γ,n)^{159}Gd		1500	923	550	7.451
^{141}Pr(γ,n)^{140}Pr	15	300	25	300	9.399
^{160}Gd(γ,n)^{159}Gd		1500	1279	554	7.451
^{162}Er(γ,n)^{161}Er		1500	279	366	9.205

different gamma ray strength functions. The cross sections are also estimated by Geant4 [6–8] Monte Carlo simulations for yield measurement using two different PhysicsLists from the code. The Geant4 simulations are also validated by simulating the standard ^{197}Au(γ,n)^{196}Au reaction cross section. The measured cross sections are in good agreement with the theoretical cross sections calculated using TALYS 1.95 and simulated cross sections using Geant4 code for some chosen gamma ray strength functions.

2 Experimental

2.1 Sample preparation

The samples were prepared from pure Pr_2O_3, Gd_2O_3 and Er_2O_3 (99.99%) in powdered form having natural isotopic abundance. For every sample, 1 gm of powder was weighed with a micro balance having an accuracy of 10 μg. The powder was wrapped in polyethylene sheet to make a cuboid of size 1 cm^3. The Au foils of the same cross-sectional area, used for bremsstrahlung flux monitoring weighed 0.5 gm each.

2.2 Irradiation

The irradiations were performed using a medical LINAC at Dr. Vikhe Patil Memorial Hospital, Ahmednagar, India. The linear accelerator was operated in photon mode, which provided 10 and 15 MeV bremsstrahlung photons. The gantry of the accelerator was pointing downwards and the collimators (jaws) were opened to give a field size of 10 × 10 cm at the patient table situated at 100 cm from the bremsstrahlung target. The samples were placed in the given field size and irradiated with 10 MeV and 15 MeV bremsstrahlung photons for a period of 300 and 1500 s. A constant dose rate of 590 ± 10 and 680 ± 10 cGy/min was maintained for 10 MeV and 15 MeV energies respectively. Along with each sample an Au sample was placed for monitoring the bremsstrahlung flux. The product of the ^{141}Pr sample has short half-life and required gamma counting as soon as possible after the irradiation. The Pr sample was pulled by a string from the irradiation table to the counting room through a pipe and with this arrangement, a low cooling time of 25 s could be made possible. For the Pr sample the irradiation lasted for 300 s while the monitor Au foil was irradiated for 1500 s. On the other hand, the Gd and Er samples were irradiated for 1500 s along with the monitor and moved to the gamma spectrometry room manually.

2.3 Measurement of gamma ray activity

The induced gamma ray activity in the irradiated samples was measured with a HPGe detector. The HPGe detector was precalibrated with a standard ^{152}Eu point γ source. The ^{152}Eu γ source has a half-life of 13.517 years [13] and had an initial activity 4336.98 Bq on 1 Oct. 1999. The efficiency for the gamma energies was obtained following our earlier works [14–17], by interpolating the equation

$$\ln(\varepsilon_i) = \sum_m p_m (\ln E_i)^{m-1} \quad (1)$$

where, ε_i are efficiencies, p_m are the fitting parameters of the order m = 5 and E_i are the corresponding gamma energies in MeV from Table 1. The fitting parameters are p_m = (− 5.0691, − 1.6275, 0.2412, 0.5790, 0.1604). The nuclear

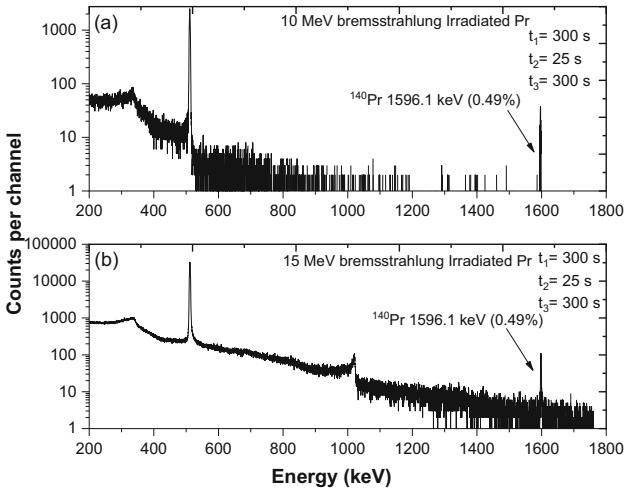

Fig. 1 Gamma ray spectra of the Pr sample irradiated with (**a**) 10 MeV bremsstrahlung photons and (**b**) 15 MeV bremsstrahlung photons

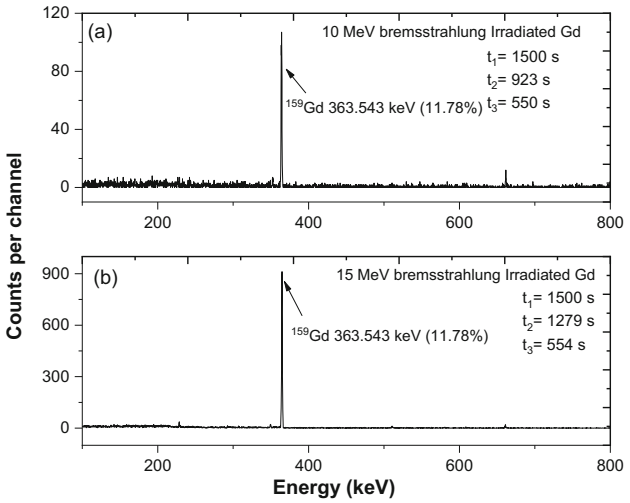

Fig. 2 Gamma ray spectra of the Gd sample irradiated with (**a**) 10 MeV bremsstrahlung photons and (**b**) 15 MeV bremsstrahlung photons

spectroscopic data for the radioisotopes produced by (γ,n) reactions is given in Table 1. The HPGe detector has a resolution of 1.5 keV at 1.33 MeV gamma peak. The HPGe crystal is p-type having radius 3.18 cm and length 4.85 cm. The output of the detector was connected to an Ortec 8 k Multi Channel Analyzer operated with Maestro software on a personal computer. The detector was lead shielded in order to reduce the background gamma rays. The activity induced in the Au sample was measured for 600 s after the accompanying sample. The experimental timing details for each sample are given in Table 2. The typical γ-ray spectra of the Pr, Gd and Er sample irradiated with bremsstrahlung photons are shown in Figs. 1, 2 and 3 respectively. The channel dispersion for the 10 MeV spectra is 0.2175 keV/channel, whereas for 15 MeV spectra it is 0.2177 keV/channel.

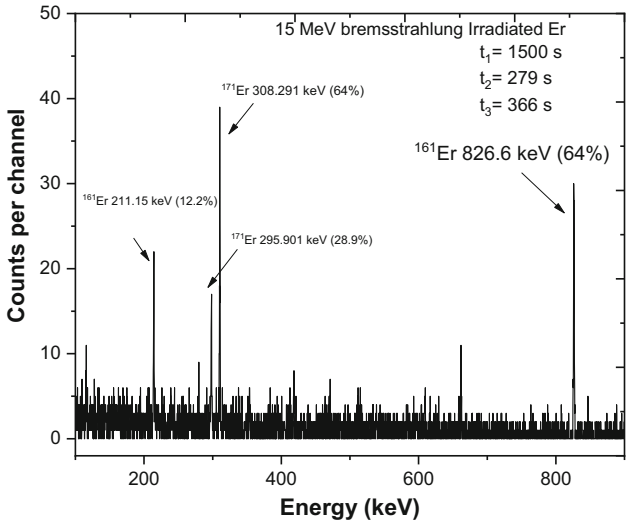

Fig. 3 Gamma ray spectrum of the Er sample irradiated with 15 MeV bremsstrahlung photons

The Er sample has six stable isotopes with mass numbers 162, 164, 166–168 and 170. However, no gamma ray, originating from the residual nuclei produced by (gamma,n) reaction on these isotopes, has been detected, except for ^{162}Er. The ^{164}Er(γ,n)^{163}Er has a finite probability of occurrence but the gamma peaks of ^{163}Er are very weak to be detected. The product of ^{166}Er(γ,n) reaction ^{165}Er has no gamma peaks in its decay scheme. Similar justification is applicable for other possible reaction ^{170}Er(γ,n)^{169}Er. So, although ^{162}Er is only 0.14% abundant, the irradiation of the other isotopes does not create a problem to extract the ^{161}Er line yields cleanly.

3 Data analysis

3.1 Estimation of bremsstrahlung flux

The estimation of incident photon flux is a crucial parameter, for the measurement of cross sections induced by photons having a continuous energy distribution. We have used Au foil along with each sample during the irradiations for monitoring the bremsstrahlung photon flux. The reaction ^{197}Au(γ,n)^{196}Au was used for the measurement of photon flux at both 10 and 15 MeV bremsstrahlung energies, as the reaction ^{197}Au(γ,n)^{196}Au has a threshold energy of 8.07 MeV. A typical γ-spectrum of the irradiated Au sample is shown in the Fig. 4. The reaction ^{197}Au(γ,n)^{196}Au is commonly used for photon flux monitoring because the product ^{196}Au has a relatively long half-life and good γ-ray intensity. The cross section data is also available on EXFOR [18–22] and evaluated data libraries [23–25]. The cross section of formation for the ^{196m2}Au is about 2 orders of magnitude less than that for the formation of ^{196}Au. Therefore, in the gamma

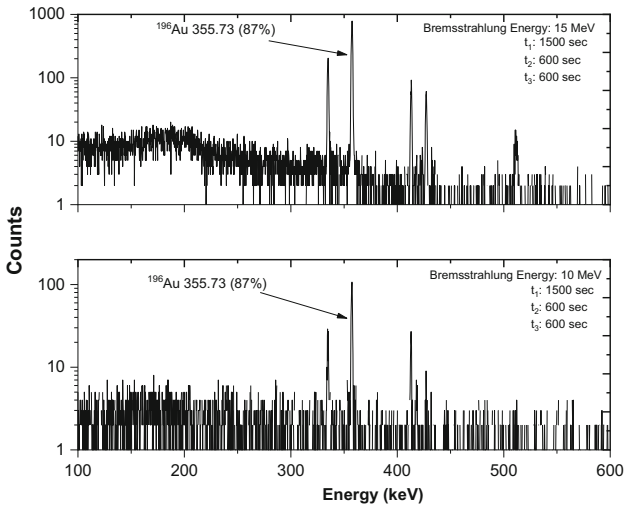

Fig. 4 A typical gamma ray spectra of the Au sample irradiated with 10 and 15 MeV bremsstrahlung photons

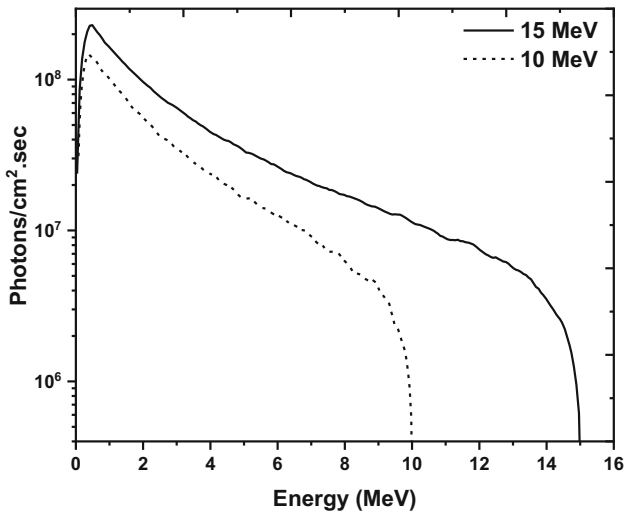

Fig. 5 Geant4 simulated bremsstrahlung spectra for 10 MeV and 15 MeV end point energies

spectrum of the irradiated natural Au foil, the gamma peaks of ^{196m2}Au were not observed. The bremsstrahlung photon flux distribution was obtained from the Geant4[6–8] Monte Carlo simulations. The gantry of the medical LINAC was accurately modeled in the Geant4 code. The photons incident on the patient table situated at 100 cm from the tungsten target were scored and normalized with the incident electron current. A standard cubic water phantom of 30 cm was simulated at the patient table. The dose deposited in the water phantom was scored and correlated with the experimental dose rate of 590 ± 10 and 680 ± 10 cGy/min for 10 MeV and 15 MeV energies respectively. The bremsstrahlung photon flux for 10 and 15 MeV end point energies are shown in Fig. 5. The cross section for the ^{197}Au(γ,n)^{196}Au reaction from the reaction threshold to 20 MeV photon energy was calculated with TALYS 1.95 code [5], using the default parameters for level density and optical model potential and the generalized Lorentzian of Brink and Axel (GSF2) for gamma strength function. The calculated cross sections with this combination of parameters agree with the evaluated data from TENDL 2019 and JENDL/PD-2016.1. The integrated bremsstrahlung photon flux for the ^{197}Au(γ,n)^{196}Au reaction can be calculated by Eq. 2,

$$< \phi_{Au} >= \frac{FA\lambda}{< \sigma_{Au} > \varepsilon I_\gamma N\left(1-e^{-\lambda t_1}\right)\left(e^{-\lambda t_2}\right)\left(1-e^{-\lambda t_3}\right)} \quad (2)$$

where, F is the activity correction factor for self-absorption and true coincidence summing, A is the area under the gamma peak, λ is the decay constant, ε is the detector efficiency, I_γ is the gamma peak intensity, N is the number of target atoms, t_1 is the irradiation time, t_2 is the time between the stop of irradiation and start of the gamma counting, t_3 is the counting time and $<\sigma_{Au}>$ is the flux weighted average cross section of ^{197}Au(γ,n)^{196}Au reaction determined by Eq. 3. The measured area under the gamma peak A is corrected for coincidence summing effect using the TrueCoinc code [26]. The factor F is the product of the self-absorption correction factor and true coincidence summing correction factor. The measured area under the gamma peak A is also corrected for the dead time of the detector by multiplying it with the ratio of clock time (CL) and live time (LT). The cross sections calculated for ^{197}Au(γ,n)^{196}Au reaction are 30.28 mb and 161.24 mb for 10 and 15 MeV bremsstrahlung photons, respectively, as calculated with Eq. 3,

$$\langle \sigma_{Au} \rangle = \frac{\sum \sigma \phi}{\sum \phi} \quad (3)$$

where ϕ is the Geant4 simulated bremsstrahlung flux and σ is the cross section of the reaction at the corresponding photon energies calculated with TALYS 1.95. The cross sections calculated using TALYS 1.95 code for GSF2 compared with TENDL 2019 and JENDL/PD-2016.1 is shown in Fig. 6, which also presents the cross section curves used by the corresponding Geant4 PhysicsLists.

3.2 Flux weighted average cross section for the (γ, n) reactions

The flux weighted average cross sections of the reactions ^{141}Pr(γ,n)^{140}Pr, ^{160}Gd(γ,n)^{159}Gd and ^{162}Er(γ,n)^{161}Er at 10 and 15 MeV bremsstrahlung end point energies were evaluated from the measured yields. The reaction ^{162}Er(γ,n)^{161}Er is measured only at 15 MeV because for 10 MeV bremsstrahlung photons the reaction yields are

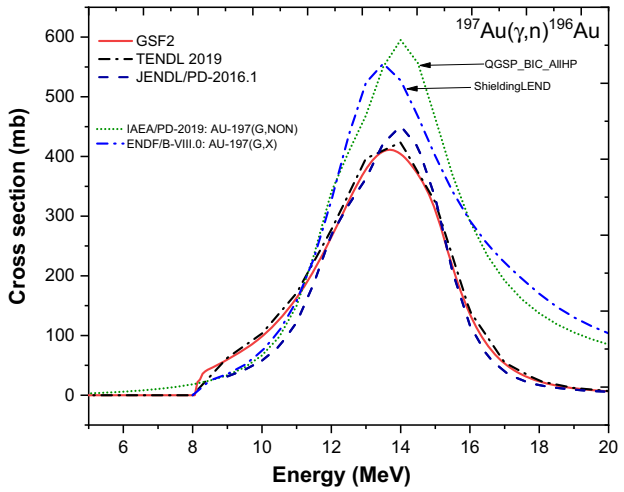

Fig. 6 The cross section of the ^{197}Au(γ,n)^{196}Au reaction calculated with the TALYS 1.95 code for GSF2 compared with the TENDL 2019, IAEA/PD-2019 and ENDF/B-VIII:0 evaluated data

practically impossible to measure due to the proximity of the threshold energy and due to the low abundance of ^{162}Er isotope. The integrated bremsstrahlung flux for the ^{197}Au(γ,n)^{196}Au monitor reaction is measured for each accompanying sample, but it cannot be directly used for the calculation of average cross section due to the difference in the threshold energies. The integrated photon flux of ^{197}Au(γ,n)^{196}Au monitor reaction needs to be corrected with the correction factor given by Eq. 4,

$$CF = \frac{\int_{E_{th,x}}^{E_e} \phi(E)dE}{\int_{E_{th,Au}}^{E_e} \phi(E)dE} \tag{4}$$

where, $E_{th,x}$ is the threshold energy for the (γ,n) nuclear reactions and $E_{th,Au}$ = 8.07 MeV is the threshold energy for the monitor reaction. The correction factors were calculated using the bremsstrahlung photon flux distribution from the Fig. 5 and corresponding threshold values from Table 2. The calculated correction factors for the (γ,n) reactions are presented in Table 3. The integrated photon flux $<\phi_x>$ for the reactions ^{141}Pr(γ,n)^{140}Pr, ^{160}Gd(γ,n)^{159}Gd and ^{162}Er(γ,n)^{161}Er can be obtained by multiplying the integrated photon flux of the monitor reaction $<\phi_{Au}>$ by the corresponding correction factors. Finally, the flux weighted average cross section $< \sigma_x >$ for the desired (γ,n) reactions can be determined with the Eq. 5,

$$< \sigma_x >= \frac{FA\lambda}{< \phi_x > \varepsilon I_\gamma N\left(1 - e^{-\lambda t_1}\right)\left(e^{-\lambda t_2}\right)\left(1 - e^{-\lambda t_3}\right)} \tag{5}$$

Table 3 Calculated correction factors for induced activity and integrated photon flux

Reaction	Endpoint energy (MeV)	Correction factor F	Flux correction factor CF
^{141}Pr(γ,n)^{140}Pr	10	1.057	0.185
^{160}Gd(γ,n)^{159}Gd		1.063	1.573
^{197}Au(γ,n)^{196}Au		1.166	1
^{141}Pr(γ,n)^{140}Pr	15	1.057	0.678
^{160}Gd(γ,n)^{159}Gd		1.063	1.207
^{162}Er(γ,n)^{161}Er		1.031	0.711
^{197}Au(γ,n)^{196}Au		1.166	1

where all the terms have the same meaning as in Eq. 2, except for $< \phi_x >$ being the corrected integrated bremsstrahlung flux.

For the ^{160}Gd(γ,n)^{159}Gd reaction, the reaction product ^{159}Gd can also be formed by the capture of photoneutrons by ^{158}Gd. The contribution of the parasitic ^{158}Gd(n,γ)^{159}Gd can be theoretically estimated by taking the ratio of the activation Eq. 1. The contribution of the (n,γ) reaction can be estimated by the ratio given by Eq. 6,

$$R = \frac{A_{(\gamma,n)}}{A_{(n,\gamma)}} = \frac{\langle\sigma\rangle_{(\gamma,n)} a_{160Gd} \langle\phi\rangle_\gamma}{\sigma_{(n,\gamma)} a_{158Gd} \phi_n} \tag{6}$$

where $A_{(\gamma,n)}$ and $A_{(n,\gamma)}$ are counts expected by (γ,n) and (n,γ) reactions, $< \sigma >$ is the cross section for corresponding reactions, a is the abundance of the isotopes and ϕ is the flux of the photons and photoneutrons. The value of R for 15 MeV is 1090 and for 10 MeV is 525, making the contribution less than ~ 0.2% to the net counts and within the uncertainty limits. Therefore, the measured counts can be considered as total counts from (γ,n) reactions.

A standard error propagation was performed for the measured cross sections [27]. The most important uncertainty contributors are the counting statistics or peak area determinations (~ 10%), integrated photon flux (~ 5%) and HPGe detector efficiency (~ 5%). The uncertainty due to gamma peak intensity is high (6–8%) in the case of ^{140}Pr and ^{161}Er and less than 1% for ^{159}Gd. The uncertainty due to the sample mass is 3.5% for ^{162}Er due to the low abundance and less than 1% for ^{141}Pr and ^{160}Gd. The uncertainties due to the timing factors t_1, t_2 and t_3 are less than 1%. The detailed uncertainties involved in the determination of cross sections of the reactions are summarized in Table 4.

Table 4 Uncertainties (%) associated with the measurement of cross sections of the nuclear reactions

Reaction	Endpoint energy (MeV)	A	N	Iγ	ε	ϕ	Total
^{141}Pr(γ,n)^{140}Pr	10	18.18	0.1	8.16	5.06	5.27	21.22
^{160}Gd(γ,n)^{159}Gd		4.4	0.88	0.42	2.96	5.32	7.57
^{141}Pr(γ,n)^{140}Pr	15	8.68	0.1	8.16	5.06	5.36	14.02
^{160}Gd(γ,n)^{159}Gd		1.39	0.88	0.42	2.96	5.24	6.25
^{162}Er(γ,n)^{161}Er		7.43	3.6	6.25	2.42	5.26	11.89

3.3 Nuclear model calculations

The theoretical nuclear model calculations for the reactions ^{141}Pr(γ,n)^{140}Pr, ^{160}Gd(γ,n)^{159}Gd, ^{162}Er(γ,n)^{161}Er and monitor reaction ^{197}Au(γ,n)^{196}Au were performed with TALYS 1.95 nuclear code [5]. The TALYS-1.95 code can be effectively used for the calculations of nuclear reaction cross sections with mono energetic projectiles such as gamma, neutrons, protons, deuterons, and α-particles in the energy range from 1 keV to 200 MeV. For the reaction ^{197}Au(γ,n)^{196}Au the default sets of parameters were used which comprise Hauser-Feshbach mechanism [28] for the compound nucleus reactions, the phenomenological Constant temperature model and the Fermi gas model (CTM + FGM) for nuclear level densities, the nucleon-nucleus optical model potentials given by the nucleus specific local optical model (KD localOMP) [29], the two-component exciton model for calculating pre-equilibrium contribution and the γ-ray transmission coefficients for E1 transition given by the Brink and Axel generalized Lorentzian [30, 31].

The theoretical cross sections for ^{141}Pr(γ,n)^{140}Pr, ^{160}Gd(γ,n)^{159}Gd and ^{162}Er(γ,n)^{161}Er reactions were performed with the same set of default parameters for nuclear level density, nucleon-nucleus optical model potential and pre-equilibrium contribution mentioned above. It was observed that the change in level density models do not majorly alter the excitation function curves. The shape of the excitation function curve mainly depends on the gamma strength functions. There are eight gamma strength functions available in the TALYS 1.95 code namely:

GSF 1: Generalized Lorentzian of Kopecky and Uhl [32]

GSF 2: Generalized Lorentzian of Brink and Axel [30, 31]

GSF 3: Hartee-Fock-BCS-quasiparticle random-phase approximation [33]

GSF 4: Hartree-Fock-Bogolyubov−quasiparticle random-phase approximation [33]

GSF 5: Hybrid model of Goriely [34]

GSF 6: Goriely T-dependent HFB [35]

GSF 7: T-dependent RMF [35]

GSF 8: Gogny D1M HFB + QRPA [35]

The calculations for theoretical effective cross sections were performed for all the eight gamma strength functions with Eq. 3. Only a few strength functions produce the values matching closely with our experimental results and these are presented in later tables.

3.4 Geant4 simulations

Geant4 is a Monte Carlo particle transport code used to simulate the interactions of radiation with matter. In the present work, we have calculated the flux weighted average cross sections of the nuclear reactions ^{141}Pr(γ,n)^{140}Pr, ^{160}Gd(γ,n)^{159}Gd and ^{162}Er(γ,n)^{161}Er using the Monte Carlo simulations by (counting) scoring the number of product radioisotopes (^{140}Pr, ^{159}Gd and ^{161}Er) formed in the simulated material. The number of product radioisotopes (referred as yield hereafter) of the nuclear reaction is related to the cross section of the nuclear reaction through the Eq. 7 [36],

$$\sigma = \frac{dN}{N \cdot n \cdot dx} \tag{7}$$

where, dN is the simulated yield of the product radioisotopes, N is the total number of bremsstrahlung photons incident, n is the number density of the target materials and dx is the thickness of the material.

In the Geant4 simulations we have simulated a cylindrical sample with 1 cm radius and 0.1 cm length along the Z axis. The materials Pr, Gd and Er of natural isotopic abundances, were assigned to the cylindrical solid in the simulations. The simulated bremsstrahlung photon spectrum from Fig. 5 was given as an input to the G4GeneralParticleSource, with photons having momentum towards the + Z direction. The bremsstrahlung photons interact with the material in the simulations through photonuclear interactions. In the SteppingAction the yield of the photonuclear interactions was scored. The cross section for the (γ,n) reaction was calculated with Eq. 7. The calculated number density, the yield of the product radioisotopes and calculated cross sections are presented in Table 5. The simulations were performed for 10^9 primary bremsstrahlung photons.

The simulations were performed with the two Physics Lists QGSP_BIC_AllHP and ShieldingLEND. The Physics List QGSP_BIC_AllHP uses the data from the IAEA PD 2019 [23] data library for photonuclear interactions which is located in the G4PARTICLEXS4.0 folder provided with the Geant4 package. The IAEA PD 2019 library consists of

Table 5 The calculated number density for the reactant isotopes, products yield calculated with Geant4 code and corresponding effective cross section

Reaction	Endpoint energy (MeV)	Number density n (atoms/cm^3)	QGSPBICAllHP		ShieldingLEND	
			dN	Cross section (mb)	dN	Cross section (mb)
^{141}Pr(γ,n)^{140}Pr	10	2.868×10^{22}	673	0.24	29,474	10.28
^{160}Gd(γ,n)^{159}Gd		6.586×10^{21}	9629	14.62	–	–
^{197}Au(γ,n)^{196}Au		5.907×10^{22}	29,761	5.04	166,003	28.10
^{141}Pr(γ,n)^{140}Pr	15	2.868×10^{22}	198,960	69.37	243,180	84.79
^{160}Gd(γ,n)^{159}Gd		6.586×10^{21}	88,521	134.39	–	–
^{162}Er(γ,n)^{161}Er		4.537×10^{19}	546	120.32	–	–
^{197}Au(γ,n)^{196}Au		5.907×10^{22}	891,616	150.92	982,338	166.28

inelastic cross sections of photonuclear interactions for all the elements and some selected isotopes. The Physics List ShieldingLEND uses the data from the ENDF-B-VIII.0 [24] library for the photonuclear interaction. However, the ENDF-B-VIII.0 library does not contain the photonuclear data for ^{160}Gd and ^{162}Er isotopes.

In order to validate the methodology used for the simulations, the average cross section of the monitor reaction ^{197}Au(γ,n)^{196}Au was first calculated from the simulations. The isotope ^{197}Au was assigned as the target material for the simulations. The average cross section for the reaction ^{197}Au(γ,n)^{196}Au for 10 MeV and 15 MeV end point bremsstrahlung photons was found to be in agreement and within the uncertainty limits, with the average cross section calculated by Eq. 3 using TALYS 1.95 data. The flux weighted average cross section calculated with TALYS 1.95 is 30.28 mb and 161.24 mb for 10 and 15 MeV bremsstrahlung photons respectively. The cross sections calculated with Geant4 simulations (Physics List ShieldingLEND) are 28.1 mb and 166.28 mb for 10 and 15 MeV bremsstrahlung photons respectively. The Physics List QGSP_BIC_AllHP underestimates the cross section for 15 MeV bremsstrahlung photons by 9% but for 10 MeV bremsstrahlung photons it underestimates the cross section by a factor of 5.6. These results suggest that this technique of Geant4 simulation can be used to determine the average cross sections of the other reactions using a proper input Physics List.

The cross section of the ^{141}Pr(γ,n)^{140}Pr reaction was calculated with both the Physics Lists. The cross section for 10 MeV bremsstrahlung photons is underestimated by a factor of 40 using Physics List QGSP_BIC_AllHP while the cross section calculated with the ShieldingLEND reasonably agrees with the TALYS and experimental data. This could be due to the interpolation tables generated by the Geant4 code and the threshold value being very close to the end point.

The cross sections for the 15 MeV bremsstrahlung photons calculated for the reactions ^{141}Pr(γ,n)^{140}Pr and ^{197}Au(γ,n)^{196}Au are underestimated using the QGSP_BIC_AllHP Physics List, whereas, those calculated with the ShieldingLEND Physics List agree with the TALYS 1.95 values and experimental data. The cross sections for ^{160}Gd(γ,n)^{159}Gd and ^{162}Er(γ,n)^{161}Er could not be calculated for the ShieldingLEND Physics List due to unavailability of the data. The results of the Geant4 simulations are presented in Table 5.

4 Results and discussion

In the present work, we have reported the cross sections of (γ,n) nuclear reactions induced by 10 and 15 MeV end point bremsstrahlung photons. The cross sections are measured relative to the ^{197}Au(γ,n)^{196}Au monitor reaction. The measured cross sections are presented along with their associated uncertainties calculated using standard error propagation method. The cross sections are compared with theoretical calculations performed with TALYS 1.95 using Hauser-Feshbach mechanism for compound nucleus reactions and eight different models for gamma strength functions. The cross sections calculated using the eight gamma strength functions vary with respect to the measured cross section. The value which is closest to the measured cross section is given in Table 6 and the other calculated values are mentioned in the following sections. The effective cross section was also calculated with the Geant4 Monte Carlo simulations and the values are compared with the measured cross sections in Table 6. In the following sections, the results for each reaction are discussed in details.

4.1 The ^{141}Pr(γ,n)^{140}Pr reaction

The TALYS 1.95 cross sections curves of the ^{141}Pr(γ,n)^{140}Pr reaction for mono energetic photons from threshold to 20 MeV are shown in Fig. 7. A few authors [37–41] have

Table 6 The measured cross sections of the nuclear reactions compared with TALYS 1.95 and Geant4 calculations

Reaction	Effective cross section at 10 MeV end point energy (mb)			Effective cross section at 15 MeV end point energy (mb)		
	Measured	TALYS 1.95	Geant4	Measured	TALYS 1.95	Geant4
^{141}Pr(γ,n)^{140}Pr	15.06 ± 2.74	16.66 (GSF4/GSF6)	10.28	86.11 ± 12.02	81.06/88.15 (GSF2/GSF7)	84.79
^{160}Gd(γ,n)^{159}Gd	13.43 ± 1.02	15.61 (GSF1)	14.62	135.08 ± 8.44	141.7 (GSF3)	134.39
^{162}Er(γ,n)^{161}Er	–	–	–	126.26 ± 15.02	125.59 (GSF1)	120.32

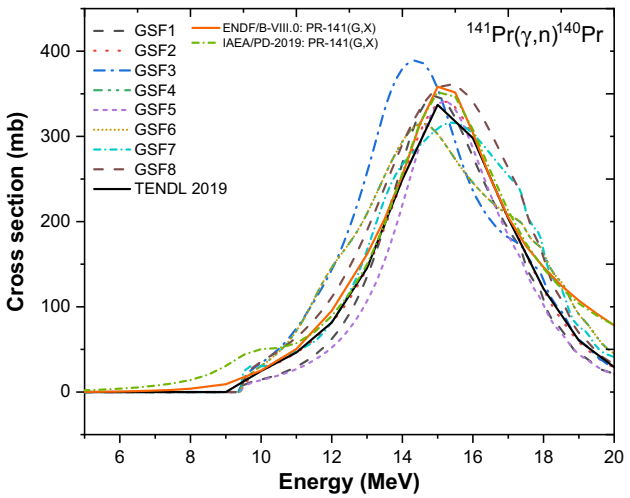

Fig. 7 The cross section of the ^{141}Pr(γ,n)^{140}Pr reaction calculated with the TALYS 1.95 code for eight different gamma strength functions compared with the TENDL 2019, IAEA/PD-2019 and ENDF/B-VIII:0 evaluated data libraries

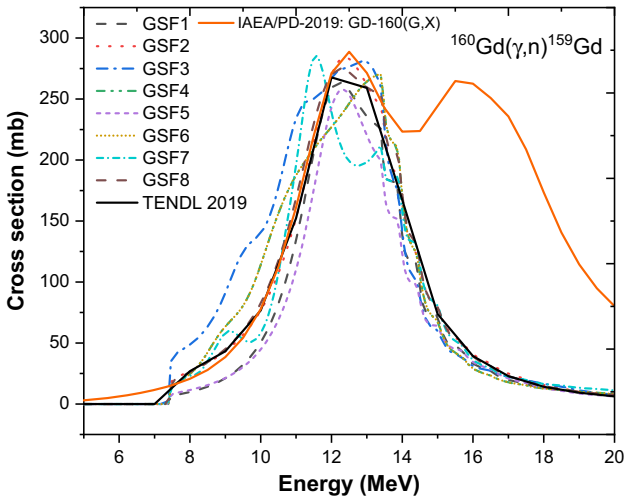

Fig. 8 The cross section of the ^{160}Gd(γ,n)^{159}Gd reaction calculated with the TALYS 1.95 code for eight different gamma strength functions compared with the TENDL 2019 and ENDF/B-VIII:0 evaluated data libraries

reported the cross sections for this reaction using mono energetic photons from 8 to 25 MeV energies. The theoretical effective cross section calculated using TALYS 1.95 for 10 MeV are 9.57, 12.76, 19.98, 16.66, 8.09, 16.66, 24.47 and 20.45 mb using GSF1 to GSF8 respectively. The corresponding calculated values for 15 MeV are 71.61, 81.06, 130.58, 113.68, 59.99, 113.67, 88.15 and 104.22 mb.

The measured flux weighted average cross section for this reaction is 15.06 ± 2.74 mb for 10 MeV and 86.12 ± 12.01 mb for 15 MeV bremsstrahlung end point energies. The experimental values agree with the calculated values with GSF4/GSF6 for 10 MeV and with GSF7 for 15 MeV. Similarly, the measured cross sections reasonably agree with the effective cross sections calculated with Geant4 using the Physics List ShieldingLEND although the Physics List QGSP_BIC_AllHP leads to discrepant results.

4.2 The ^{160}Gd(γ,n)^{159}Gd reaction

The TALYS 1.95 cross sections curves of the ^{160}Gd(γ,n)^{159}Gd reaction for mono energetic photons from threshold to 20 MeV are shown in Fig. 8. Dreyer et al. [42] and Berman et al. [43] have reported the cross section for this reaction for mono energetic photons from 7.24 to 29.2 MeV. Ghosh et al. [3] have reported the effective cross section of 38.829 ± 2.068 mb for this reaction for 10 MeV bremsstrahlung photons. This value is much higher than our result at 10 MeV, viz., 13.43 mb. However, our measurement and that of Ghosh et al. agree with the TALYS calculation with GSF1 and GSF2, respectively. The TALYS calculations for GSF1 to GSF8 15.61, 34.53, 68.32, 41.96, 16.34, 41.96, 34.65, 35.02 mb for 10 MeV and are 86.64, 106.17, 141.70, 116.11, 78.98, 116.11, 103.01, 109.80 mb for 15 MeV bremsstrahlung. In 15 MeV case, our experimental result of 135.08 mb agrees with TALYS calculation with GSF3.

The effective cross section calculated with Geant4 is 14.62 mb and 134.40 mb for 10 and 15 MeV energies respectively which is also in agreement with the measured cross section values. For the Geant4 simulations the cross section is calculated only with the QGSP_BIC_AllHP Physics List due to unavailability of data in the ENDF-B-VIII.0 library.

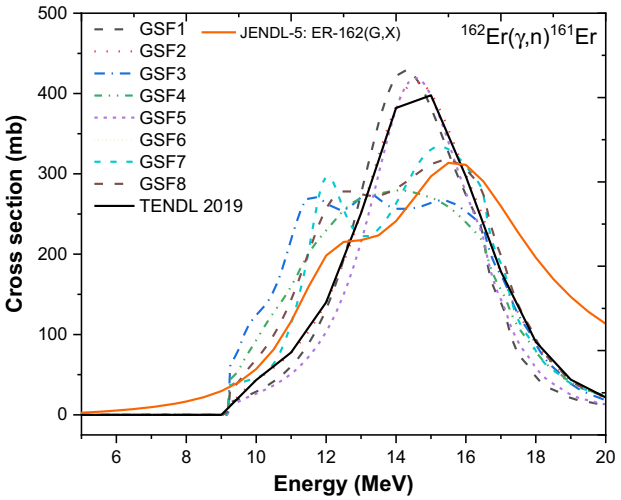

Fig. 9 The cross section of the ^{162}Er(γ,n)^{161}Er reaction calculated with the TALYS 1.95 code for eight different gamma strength functions compared with the TENDL 2019 and JENDL-5 evaluated data libraries

4.3 The ^{162}Er(γ,n)^{161}Er reaction

Figure 9 shows the cross sections curves calculated with TALYS 1.95 code for the ^{162}Er(γ,n)^{161}Er reaction for mono energetic photons from threshold to 20 MeV. Vagena et al. [4] have reported the effective cross section of 87 ± 14 mb using 14 MeV end point bremsstrahlung photons. The theoretical effective cross section calculated with TALYS 1.95 for 15 MeV are 125.59, 128.68, 197.1, 170.7, 106.13, 170.7, 149.98 and 165.35 mb for GSF1 to GSF8 respectively. This reaction is not induced by 10 MeV bremsstrahlung photons probably due to low abundance of the ^{162}Er isotope and threshold energy being very close to 10 MeV.

The measured flux weighted average cross section for this reaction is 126.26 ± 15.02 mb for 15 MeV bremsstrahlung end point energy. This agrees with TALYS calculation with GSF1. The effective cross section calculated with Geant4 is 120.32 mb for 15 MeV energy which is in agreement with the measured cross section value. For the Geant4 simulations the cross section is calculated only with the QGSP_BIC_AllHP Physics List due to unavailability of data in the ENDF-B-VIII.0 library.

From all the results discussed above, it is apparent that, the effective cross section is dependent upon multiple factors such as threshold energy of the reaction, the bremsstrahlung photon flux function and the Lorentzian function defined by the gamma strength functions (GSFs). Ideally there must be an agreement between the experiment and the calculation for the same GSF used for a specific isotope, but after 10 MeV the shape of the Lorentzian function changes considerably for different GSFs and the number of bremsstrahlung photons reduces towards the end point energy. Therefore, in the present work, the measured cross section agrees with different GSF at 10 and 15 MeV energies. This indicates that it is not possible to extract information on the details of the GSF from measurements with bremsstrahlung photons at only a few end-point energies.

The Geant4 Monte Carlo simulations can be used for evaluation of cross sections of the nuclear reactions induced by radiations with complex energy spectrum. The simulation results are however dependent on the availability of the evaluated nuclear data from standard data libraries. Moreover, the evaluated data is distributed in various formats such as ENDF, GIDI, GND, etc. The Geant4 physics list shieldingLEND uses the latest data from the ENDF-B-VIII.0, which is converted to GND in xml format. The physics list QGSP_BIC_AllHP uses the data from another evaluated data library IAEA PD 2019 in tabular format converted from IAEA ENDFL-6 data files. The codes such as FUDGE [44] can convert the data from ENDF format to GND (xml) format. If the evaluated data is available in the desired format, then the simulations can be compared for different evaluated data. There is also a need to internationally adopt a single nuclear data format for intercomparison and use with different nuclear physics simulations. Such simulations are important for feasibility studies prior to an experiment being performed and also for the validation of experimental results.

5 Conclusion

The flux weighted average cross sections for the reactions ^{141}Pr(γ,n)^{140}Pr, ^{160}Gd(γ,n)^{159}Gd and ^{162}Er(γ,n)^{161}Er are reported for 10 and 15 MeV bremsstrahlung end point energies. The reported values are presented along with the associated uncertainties and the induced activity is corrected for self-absorption and true coincidence summing. The cross sections for these reactions are reported for the first time at these energies. The reported values are compared with the theoretically calculated effective cross sections using TALYS 1.95 code for eight different gamma strength functions. The effective cross sections are also calculated using Geant4 Monte Carlo code and compared with the measured values. The theoretical cross sections are a good reference for experimental results. The technique of calculating effective cross section using a Monte Carlo code by scoring the reaction yield could prove useful for future experiments. This technique can be used for other radiation induced nuclear reactions, having a continuous input energy spectrum. The results obtained with this technique are highly dependent on the availability of the evaluated data from the libraries. The measured cross sections are in agreement with theoretical calculations done with a few specific gamma ray strength functions. There are some disagreements between the measured and calculated cross sections using different GSFs majorly

due to the continuous nature of the incident bremsstrahlung photons, the Lorentzian function defined by the GSFs and the proximity of the threshold to the end point energies. The cross sections are useful for nuclear database and nuclear astrophysics study of stellar photoneutron rates.

Acknowledgements The authors [S. D. Dhole and V. N. Bhoraskar] are thankful to SERB-DST sanction number: EMR/2017/002497 and DAE-BRNS sanction number: 36(6)/14/49/2016-BRNS for the financial support. Authors are grateful to Dr. Bhushan Nikam and the management of Dr. Vikhe Patil Memorial Hospital, Ahmednagar, India for availing the medical LINAC for the experiment.

Data availability This manuscript has no associated data or the data will not be deposited. [Authors' comment: The authors declare that all data generated or analysed during this study are included in this published article.]

References

1. N. Otuka, E. Dupont, V. Semkova, B. Pritychenko, A.I. Blokhin, M. Aikawa, S. Babykina, M. Bossant, G. Chen, S. Dunaeva, R.A. Forrest, T. Fukahori, N. Furutachi, S. Ganesan, Z. Ge, O.O. Gritzay, M. Herman, S. Hlavač, K. Katō, B. Lalremruata, Y.O. Lee, A. Makinaga, K. Matsumoto, M. Mikhaylyukova, G. Pikulina, V.G. Pronyaev, A. Saxena, O. Schwerer, S. P. Simakov, N. Soppera, R. Suzuki, S. Takács, X. Tao, S. Taova, F. Tárkányi, V.V. Varlamov, J. Wang, S.C. Yang, V. Zerkin, Y. Zhuang, Nucl. Data Sheets **120**, 272 (2014)
2. D. Bandyopadhyay, K. Kar, in ed. by D. Bandyopadhyay, K. Kar (Springer International Publishing, Cham, 2022), pp. 169–202
3. R. Ghosh, S. Badwar, B. Lawriniang, S.S. Yerraguntla, H. Naik, Y. Naik, S.V. Suryanarayana, B. Jyrwa, S. Ganesan, J. Radioanal. Nucl. Chem. **314**, 1983 (2017)
4. E. Vagena, S. Stoulos, Nucl. Phys. A **957**, 259 (2017)
5. A.J. Koning, D. Rochman, Nucl. Data Sheets **113**, 2841 (2012)
6. J. Allison, K. Amako, J. Apostolakis, H. Araujo, P.A. Dubois, M. Asai, G. Barrand, R. Capra, S. Chauvie, R. Chytracek, G.A.P. Cirrone, G. Cooperman, G. Cosmo, G. Cuttone, G.G. Daquino, M. Donszelmann, M. Dressel, G. Folger, F. Foppiano, J. Generowicz, V. Grichine, S. Guatelli, P. Gumplinger, A. Heikkinen, I. Hrivnacova, A. Howard, S. Incerti, V. Ivanchenko, T. Johnson, F. Jones, T. Koi, R. Kokoulin, M. Kossov, H. Kurashige, V. Lara, S. Larsson, F. Lei, O. Link, F. Longo, M. Maire, A. Mantero, B. Mascialino, I. McLaren, P. M. Lorenzo, K. Minamimoto, K. Murakami, P. Nieminen, L. Pandola, S. Parlati, L. Peralta, J. Perl, A. Pfeiffer, M.G. Pia, A. Ribon, P. Rodrigues, G. Russo, S. Sadilov, G. Santin, T. Sasaki, D. Smith, N. Starkov, S. Tanaka, E. Tcherniaev, B. Tome, A. Trindade, P. Truscott, L. Urban, M. Verderi, A. Walkden, J.P. Wellisch, D. C. Williams, D. Wright, H. Yoshida, IEEE Trans. Nucl. Sci. **53**, 270 (2006)
7. J. Allison, K. Amako, J. Apostolakis, P. Arce, M. Asai, T. Aso, E. Bagli, A. Bagulya, S. Banerjee, G. Barrand, B.R. Beck, A.G. Bogdanov, D. Brandt, J. M.C. Brown, H. Burkhardt, Ph. Canal, D. Cano-Ott, S. Chauvie, K. Cho, G. A.P. Cirrone, G. Cooperman, M.A. Cortés-Giraldo, G. Cosmo, G. Cuttone, G. Depaola, L. Desorgher, X. Dong, A. Dotti, V.D. Elvira, G. Folger, Z. Francis, A. Galoyan, L. Garnier, M. Gayer, K.L. Genser, V.M. Grichine, S. Guatelli, P. Guèye, P. Gumplinger, A.S. Howard, I. Hřivnáčová, S. Hwang, S. Incerti, A. Ivanchenko, V.N. Ivanchenko, F.W. Jones, S.Y. Jun, P. Kaitaniemi, N. Karakatsanis, M. Karamitros, M. Kelsey, A. Kimura, T. Koi, H. Kurashige, A. Lechner, S.B. Lee, F. Longo, M. Maire, D. Mancusi, A. Mantero, E. Mendoza, B. Morgan, K. Murakami, T. Nikitina, L. Pandola, P. Paprocki, J. Perl, I. Petrović, M. G. Pia, W. Pokorski, J. M. Quesada, M. Raine, M. A. Reis, A. Ribon, A. Ristić Fira, F. Romano, G. Russo, G. Santin, T. Sasaki, D. Sawkey, J.I. Shin, I.I. Strakovsky, A. Taborda, S. Tanaka, B. Tomé, T. Toshito, H.N. Tran, P.R. Truscott, L. Urban, V. Uzhinsky, J.M. Verbeke, M. Verderi, B.L. Wendt, H. Wenzel, D.H. Wright, D.M. Wright, T. Yamashita, J. Yarba, H. Yoshida, Nucl. Instrum. Methods Phys. Res. A **835**, 186 (2016)
8. S. Agostinelli, J. Allison, K. Amako, J. Apostolakis, H. Araujo, P. Arce, M. Asai, D. Axen, S. Banerjee, G. Barrand, F. Behner, L. Bellagamba, J. Boudreau, L. Broglia, A. Brunengo, H. Burkhardt, S. Chauvie, J. Chuma, R. Chytracek, G. Cooperman, G. Cosmo, P. Degtyarenko, A. Dell'Acqua, G. Depaola, D. Dietrich, R. Enami, A. Feliciello, C. Ferguson, H. Fesefeldt, G. Folger, F. Foppiano, A. Forti, S. Garelli, S. Giani, R. Giannitrapani, D. Gibin, J.J. Gómez Cadenas, I. González, G. Gracia Abril, G. Greeniaus, W. Greiner, V. Grichine, A. Grossheim, S. Guatelli, P. Gumplinger, R. Hamatsu, K. Hashimoto, H. Hasui, A. Heikkinen, A. Howard, V. Ivanchenko, A. Johnson, F.W. Jones, J. Kallenbach, N. Kanaya, M. Kawabata, Y. Kawabata, M. Kawaguti, S. Kelner, P. Kent, A. Kimura, T. Kodama, R. Kokoulin, M. Kossov, H. Kurashige, E. Lamanna, T. Lampén, V. Lara, V. Lefebure, F. Lei, M. Liendl, W. Lockman, F. Longo, S. Magni, M. Maire, E. Medernach, K. Minamimoto, P. Mora de Freitas, Y. Morita, K. Murakami, M. Nagamatu, R. Nartallo, P. Nieminen, T. Nishimura, K. Ohtsubo, M. Okamura, S. O'Neale, Y. Oohata, K. Paech, J. Perl, A. Pfeiffer, M.G. Pia, F. Ranjard, A. Rybin, S. Sadilov, E. di Salvo, G. Santin, T. Sasaki, N. Savvas, Y. Sawada, S. Scherer, S. Sei, V. Sirotenko, D. Smith, N. Starkov, H. Stoecker, J. Sulkimo, M. Takahata, S. Tanaka, E. Tcherniaev, E. Safai Tehrani, M. Tropeano, P. Truscott, H. Uno, L. Urban, P. Urban, M. Verderi, A. Walkden, W. Wander, H. Weber, J.P. Wellisch, T. Wenaus, D.C. Williams, D. Wright, T. Yamada, H. Yoshida, D. Zschiesche, Nucl. Instrum. Methods Phys. Res. A **506**, 250 (2003)
9. N. Nica, Nucl. Data Sheets **154**, 1 (2018)
10. H. Xiaolong, Nucl. Data Sheets **108**, 1093 (2007)
11. C.W. Reich, Nucl. Data Sheets **112**, 2497 (2011)
12. C.W. Reich, Nucl. Data Sheets **113**, 157 (2012)
13. M.J. Martin, Nucl. Data Sheets **114**, 1497 (2013)
14. G.T. Bholane, T.S. Ganesapandy, A.B. Phatangare, F.M.D. Attar, S.S. Dahiwale, S.V. Suryanarayana, V.N. Bhoraskar, S.D. Dhole, Nucl. Phys. A **1020**, 122399 (2022)
15. G.T. Bholane, T.S. Ganesapandy, A.B. Phatangare, F.M.D. Attar, S.S. Dahiwale, S.V. Suryanarayana, V.N. Bhoraskar, S.D. Dhole, Radiat. Phys. Chem. **195**, 1 (2022)
16. T.S. Ganesapandy, G.T. Bholane, A.B. Phatangare, F.M.D. Attar, S.S. Dahiwale, S.V. Suryanarayana, V.N. Bhoraskar, S.D. Dhole, Eur. Phys. J. Plus **137**, 711 (2022)
17. G.T. Bholane, T.S. Ganesapandy, A.B. Phatangare, V.D. Bharud, B.J. Patil, S.S. Dahiwale, S.V. Suryanarayana, V.N. Bhoraskar, S.D. Dhole, Appl. Radiat. Isotopes **174**, 109739 (2021)
18. H. Naik, G. Kim, K. Kim, M. Zaman, A. Goswami, M.W. Lee, S.C. Yang, Y.O. Lee, S.G. Shin, M.H. Cho, Nucl. Phys. A **948**, 28 (2016)
19. M.S. Rahman, K.S. Kim, M. Lee, G. Kim, Y. Oh, H.S. Lee, M.H. Cho, I.S. Ko, W. Namkung, V. do Nguyen, D.K. Pham, T.T. Kim, T.I. Ro, J. Radioanal. Nucl. Chem. **283**, 519 (2010)
20. K.Y. Hara, H. Harada, F. Kitatani, S. Goko, S.Y. Hohara, T. Kaihori, A. Makinaga, H. Utsunomiya, H. Toyokawa, K. Yamada, J. Nucl. Sci. Technol. **44**, 938 (2007)
21. F. Kitatani, H. Harada, S. Goko, H. Utsunomiya, H. Akimune, T. Kaihori, H. Toyokawa, K. Yamada, J. Nucl. Sci. Technol. **47**, 367 (2010)

22. C. Plaisir, F. Hannachi, F. Gobet, M. Tarisien, M.M. Aléonard, V. Méot, G. Gosselin, P. Morel, B. Morillon, Eur. Phys. J. A **48**, 1 (2012)
23. T. Kawano, Y.S. Cho, P. Dimitriou, D. Filipescu, N. Iwamoto, V. Plujko, X. Tao, H. Utsunomiya, V. Varlamov, R. Xu, R. Capote, I. Gheorghe, O. Gorbachenko, Y.L. Jin, T. Renstrøm, M. Sin, K. Stopani, Y. Tian, G.M. Tveten, J.M. Wang, T. Belgya, R. Firestone, S. Goriely, J. Kopecky, M. Krtička, R. Schwengner, S. Siem, M. Wiedeking, Nucl. Data Sheets **163**, 109 (2020)
24. D.A. Brown, M.B. Chadwick, R. Capote, A.C. Kahler, A. Trkov, M.W. Herman, A.A. Sonzogni, Y. Danon, A.D. Carlson, M. Dunn, D.L. Smith, G.M. Hale, G. Arbanas, R. Arcilla, C.R. Bates, B. Beck, B. Becker, F. Brown, R.J. Casperson, J. Conlin, D.E. Cullen, M.-A. Descalle, R. Firestone, T. Gaines, K.H. Guber, A.I. Hawari, J. Holmes, T.D. Johnson, T. Kawano, B.C. Kiedrowski, A.J. Koning, S. Kopecky, L. Leal, J.P. Lestone, C. Lubitz, J.I. Márquez Damián, C.M. Mattoon, E.A. McCutchan, S. Mughabghab, P. Navratil, D. Neudecker, G.P.A. Nobre, G. Noguere, M. Paris, M.T. Pigni, A.J. Plompen, B. Pritychenko, V.G. Pronyaev, D. Roubtsov, D. Rochman, P. Romano, P. Schillebeeckx, S. Simakov, M. Sin, I. Sirakov, B. Sleaford, V. Sobes, E.S. Soukhovitskii, I. Stetcu, P. Talou, I. Thompson, S. van der Marck, L. Welser-Sherrill, D. Wiarda, M. White, J. L. Wormald, R.Q. Wright, M. Zerkle, G. Žerovnik, Y. Zhu. Nucl. Data Sheets **148**, 1 (2018)
25. A.J. Koning, D. Rochman, J.Ch. Sublet, N. Dzysiuk, M. Fleming, S.C. van der Marck, O.V. Bogdankevich, L.E. Lazareva, F.A. Nikolaev, D. Rochman, A.J. Koning, J.Ch. Sublet, M. Fleming, E. Bauge, S. Hilaire, P. Romain, B. Morillon, H. Duarte, S. Goriely, S.C. van der Marck, H. Sjöstrand, S. Pomp, N. Dzysiuk, O. Cabellos, H. Ferroukhi, A. Vasiliev, S. Agostinelli, J. Allison, K. Amako, J. Apostolakis, H. Araujo, P. Arce, M. Asai, D. Axen, S. Banerjee, G. Barrand, F. Behner, L. Bellagamba, J. Boudreau, L. Broglia, A. Brunengo, H. Burkhardt, S. Chauvie, J. Chuma, R. Chytracek, G. Cooperman, G. Cosmo, P. Degtyarenko, A. Dellcqua, G. Depaola, D. Dietrich, R. Enami, A. Feliciello, C. Ferguson, H. Fesefeldt, G. Folger, F. Foppiano, A. Forti, S. Garelli, S. Giani, R. Giannitrapani, D. Gibin, J.J. Gómez Cadenas, I. González, G. Gracia Abril, G. Greeniaus, W. Greiner, V. Grichine, A. Grossheim, S. Guatelli, P. Gumplinger, R. Hamatsu, K. Hashimoto, H. Hasui, A. Heikkinen, A. Howard, V. Ivanchenko, A. Johnson, F.W. Jones, J. Kallenbach, N. Kanaya, M. Kawabata, Y. Kawabata, M. Kawaguti, S. Kelner, P. Kent, A. Kimura, T. Kodama, R. Kokoulin, M. Kossov, H. Kurashige, E. Lamanna, T. Lampén, V. Lara, V. Lefebure, F. Lei, M. Liendl, W. Lockman, F. Longo, S. Magni, M. Maire, E. Medernach, K. Minamimoto, P. Mora de Freitas, Y. Morita, K. Murakami, M. Nagamatu, R. Nartallo, P. Nieminen, T. Nishimura, K. Ohtsubo, M. Okamura, S. O'Neale, Y. Oohata, K. Paech, J. Perl, A. Pfeiffer, M.G. Pia, F. Ranjard, A. Rybin, S. Sadilov, E. di Salvo, G. Santin, T. Sasaki, N. Savvas, Y. Sawada, S. Scherer, S. Sei, V. Sirotenko, D. Smith, N. Starkov, H. Stoecker, J. Sulkimo, M. Takahata, S. Tanaka, E. Tcherniaev, E. Safai Tehrani, M. Tropeano, P. Truscott, H. Uno, L. Urban, P. Urban, M. Verderi, A. Walkden, W. Wander, H. Weber, J.P. Wellisch, T. Wenaus, D.C. Williams, D. Wright, T. Yamada, H. Yoshida, D. Zschiesche, A.J. Koning, D. Rochman, J.C. Sublet, N. Dzysiuk, M. Fleming, S.C. van der Marck, Nucl. Data Sheets **506**, 250 (2019)
26. S. Sudar, in *"TrueCoinc" Software Utility for Calculation of the True Coincidence Correction* (International Atomic Energy Agency (IAEA), 2002).
27. N. Otuka, B. Lalremruata, M.U. Khandaker, A.R. Usman, L.R.M. Punte, Radiat. Phys. Chem. **140**, 502 (2017)
28. W. Hauser, H. Feshbach, Phys. Rev. **87**, 366 (1952)
29. A.J. Koning, J.P. Delaroche, Nucl. Phys. A **713**, 231 (2003)
30. D. Brink, Nucl. Phys. **4**, 215 (1957)
31. P. Axel, Phys. Rev. **126**, 671 (1962)
32. J. Kopecky, M. Uhl, Phys. Rev. C **41**, 1941 (1990)
33. S. Goriely, F. Tondeur, J.M. Pearson, At. Data Nucl. Data Tables **77**, 311 (2001)
34. S. Goriely, Phys. Lett. B **436**, 10 (1998)
35. S. Goriely, S. Hilaire, A.J. Koning, Phys. Rev. C **78**, 64307 (2008)
36. L.F. Curtiss, G.B. Beard, Am. J. Phys. **27**, 528 (1959)
37. B.L. Berman, R.E. Pywell, S.S. Dietrich, M.N. Thompson, K.G. McNeill, J.W. Jury, Phys. Rev. C **36**, 1286 (1987)
38. B.C. Cook, D.R. Hutchinson, R.C. Waring, J.N. Bradford, R.G. Johnson, J.E. Griffin, Phys. Rev. **143**, 730 (1966)
39. W.E. del Bianco, W.E. Stephens, Phys. Rev. **126**, 709 (1962)
40. R.E. Sund, V.V. Verbinski, H. Weber, L.A. Kull, Phys. Rev. C **2**, 1129 (1970)
41. H. Utsunomiya, A. Makinaga, S. Goko, T. Kaihori, H. Akimune, T. Yamagata, M. Ohta, H. Toyokawa, S. Müller, Y.W. Lui, S. Goriely, Phys. Rev. C Nucl. Phys. **74**, 025806 (2006)
42. F. Dreyer, H. Dahmen, J. Staude, H.H. Thies, Nucl. Phys. Sect. A **192**, 433 (1972)
43. B.L. Berman, M.A. Kelly, R.L. Bramblett, J.T. Caldwell, H.S. Davis, S.C. Fultz, Phys. Rev. **185**, 1576 (1969)
44. C.M. Mattoon, B.R. Beck, N.R. Patel, N.C. Summers, G.W. Hedstrom, D.A. Brown, Nucl. Data Sheets **113**, 3145 (2012)